Convective Transport about Cylinder with Surface Reaction of Arbitrary Order

Hoa D. Nguyen, Seungho Paik, and Rod W. Douglass
Idaho National Engineering Laboratory, Idaho Falls, ID 83415

Heat and mass transfer from a circular cylinder exposed to a convective environment with a surface reaction of arbitrary order is studied based on the stream function-vorticity formulation. A hybrid numerical scheme combining the Fourier spectral method in the angular direction and the spectral element method in the radial direction is used to solve the conservation equations along with an influence matrix technique to resolve the vorticity boundary conditions. Results showing the temporal evolution of the flow, temperature and concentration fields are presented for cases with and without vortex shedding with the latter triggered by the cylinder's rotation. A parametric study is also performed to examine the influence of the Reynolds number, Grashof number, Prandtl number, Schmidt number, Damköhler number, the reaction order, the flow alignment, the heat of reaction, the rotational velocity and the flow pulsation on the effectiveness of the reaction surface. With the exception rotation, they all exhibit strong dependence.

Introduction

Convective heat and mass transfer associated with a catalytic body have been encountered in a number of applications where the primary function of a catalyst is to lower the activation energy, thereby, creating a favorable condition for thermodynamically legible reactions to take place at an appreciable rate. Examples include the catalytic surface recombination of atoms and the packed tubular-wall reactor.

Though transport processes in the presence of a surface-catalyzed reaction is an important class of chemically reacting flows, research in this area is somewhat limited in scope compared to those involving homogeneous reactions. Bauer (1976) considered a parabolic flow of reactant between two parallel plates subject to a first-order irreversible chemical reaction in the fluid phase as well as at the walls. In his study, the fluid was assumed isothermal and only transverse molecular diffusion was taken into account so that the species equation is simplified to a form which admits a closed-form solution. The same problem was recently treated by Basic and Dudukovic (1991) who derived an analytical expression for the concentration distribution in Leveque's approximations. In this approach, the axial velocity in the concentration boundary layer was approximated as a linear function of the transverse coordinate which is justifiable as long as the Schmidt number is sufficiently large. Physically, this is nothing more than assuming the hydrodynamic boundary layer to develop faster than the concentration counterpart. Perhaps, the novelty of their article is a demonstration of how such a solution can be adapted to pipe and film flow of power-law fluids. For flows involving more complex heterogeneous reactions, Solbrig and Gidaspow (1968) studied mass transfer in turbulent flow inside a flat duct with an n-th order surface reaction. Consecutive irreversible first-order reaction was considered by Hudson (1965) for a plug flow in a pipe and by Lyczkowski et al. (1971) for fully developed laminar flow between parallel plates and turbulent flow in a round tube. Ghez (1978) dealt with the case of a first-order reversible reaction in the framework of Leveque's approximations.

The above citations are analytical and the solutions are thus subjected to limitations as a result of the assumptions that allow for solving only the species conservation equation with an elementary flow field. More sophisticated treatments can be found in a related field wherein the flow and concentration resistances are confined primarily in thin layers next to the solid surface. By applying boundary-layer approximations and introducing similarity variables, the flow equations become the Blasius boundary layer equations and the resulting velocity is used to determine the species concentration (Riley, 1972). Excellent authoritative reviews of the literature

Correspondence concerning this article should be addressed to H. D. Nguyen.

were provided by Rosner (1964) and Chung (1965) with the latter covering thermal effects as well. Even though the solutions obtained from this approach are useful in their own right, they are only valid when the velocity is high enough to warrant the existence of boundary layers. In addition, the chemistry in these problems was assumed such that the forward and reverse rates were equal at all times. Smith and Carberry (1975) and Finlayson (1978) performed numerical simulations in which temperature and concentration are coupled at the tube surface with experimentally derived reaction kinetics and a known velocity. Finlayson (1978) reported the existence of a multiplicity of steady states for wall-catalyzed oxidation of carbon monoxide and concluded that a past knowledge of reactor operations is necessary for determining the actual one.

It is clear that the aforementioned treatments of the transport phenomena in the presence of a surface reaction are somewhat oversimplified. More often than not, the velocity is not known *a priori* and chemically generated heating effects may not be negligible; therefore, a more rigorous approach wherein the momentum, energy, and species equations must be solved simultaneously would be desirable. The purpose of this study is to investigate the problem including the internal heat conduction in order to establish a fundamental understanding about the nature of simultaneous interactions of convection, diffusion, and heterogeneous reaction. Specifically, we shall consider a physical setting in which three modes of convection including the rotation of the cylinder itself, the external oscillatory flow, and the buoyancy-induced flow exist. Here, the rotation will allow us to investigate the transport processes under vortex shedding conditions while oscillation in the free-stream velocity is included to resemble turbulent flows where a large part of the unsteadiness comes from the fluctuations in the free-stream velocity. Concurrently, a nonequilibrium irreversible reaction of arbitrary order takes place along the surface of a cylinder. The results obtained from numerical simulations will be interpreted to identify the importance of various mechanisms of the heat and mass transfer.

Formulation

Problem statement

Consider the physical system depicted in Figure 1 which consists of a catalyst rod of circular cross section with radius R exposed to a reactant/carrier fluid mixture of infinite extent. Initially, the fluid itself is at rest and the fluid and catalyst are at the same temperature, T_0. Suddenly, the fluid acquires, in an impulsively started fashion, a flow velocity of mean magnitude U_∞ at an angle δ with gravity, which fluctuates in time as described by $U_\infty[1+\phi\sin(2\pi\omega_f t)]$ with ω_f and ϕ being the oscillation frequency and amplitude, respectively. In the same manner, the cylinder attains its rotational speed γ instantaneously using a convention that a positive value corresponds to counterclockwise rotation. As the reactant A comes in contact with the cylinder surface, it transforms to a new chemical species B; the reaction is symbolized as

$$A \xrightarrow{k''} B.$$

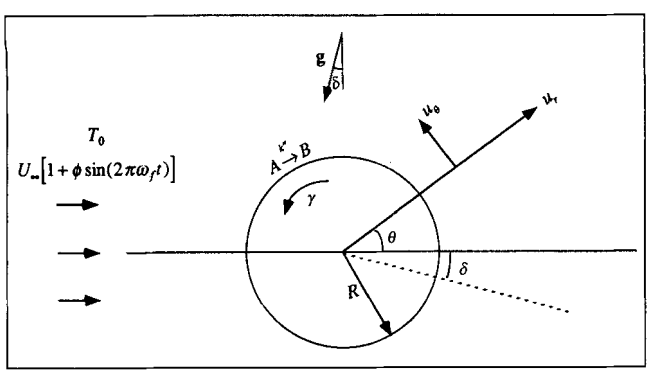

Figure 1. Physical system.

During the course of reaction, energy can either be liberated or consumed depending on whether the reaction is exothermic or endothermic. Regardless of the nature of the reaction, the temperature and the species concentration will deviate from their prescribed initial uniform state. Such nonuniformities will result in a density variation which consequently gives rise to an additional mode of convective transport driven by the buoyancy force. Unless the temperature range in the system is sufficiently small, this induced motion could lead to complex flow fields when superimposed on the main flow. As demonstrated in a recent study of Nguyen et al. (1995), the angle between the free-stream velocity and the gravity as well as the ratio Gr/Re^2 are the primary controlling factors which dictate the overall flow structure. Accordingly, heat and mass transfer may significantly be enhanced or degraded if the two convective streams cooperate or oppose each other, respectively. The reaction at the surface will be affected by the buoyancy induced flow.

The nonlinearities in the partial differential equations and the inherent couplings among them make modeling a difficult task. In addition, the reaction at the surface also poses another difficulty for the boundary conditions. In view of these complexities, we shall idealize our conceptual model with the following simplifications: (1) Oberbeck-Boussinesq approximations are valid, that is, the fluid is Newtonian with constant properties except density in the body force term where it varies as a linear function of temperature and concentration; (2) the length of the rod is much greater than its diameter so that end effects can safely be ignored (the transport processes are two-dimensional in r and θ); (3) the surface reaction is n-th order and irreversible with its rate constant obeying Arrhenius law; (4) catalicity remains constant throughout the course of the reaction; (5) thermophysical properties and transport coefficients of both reactant and product are the same; (6) constant moles or dilute solution.

Fundamental equations

Under the assumptions stated in the foregoing section, the evolution of the physicochemical process described above can be predicted from a set of simplified conservation equations including the total mass continuity equation, the Navier-Stokes equations, the energy equation, and the species equation. In mathematical form, they are given by

$$\nabla\cdot\boldsymbol{u}=0, \tag{1}$$

$$\rho\left[\frac{\partial \boldsymbol{u}}{\partial t}+\boldsymbol{u}\cdot\nabla\boldsymbol{u}\right]=-\nabla p+\mu\nabla^2\boldsymbol{u}+\rho\boldsymbol{g}, \tag{2}$$

$$\frac{\partial T}{\partial t}+\boldsymbol{u}\cdot\nabla T=\alpha\nabla^2 T, \tag{3}$$

$$\frac{\partial X}{\partial t}+\boldsymbol{u}\cdot\nabla X=D\nabla^2 X, \tag{4}$$

for the fluid phase and

$$\frac{\partial \hat{T}}{\partial t}=\hat{\alpha}\nabla^2\hat{T} \tag{5}$$

for the solid phase, hereafter distinguished by a hat.

In the above equations, D is the mass diffusion coefficient, $\boldsymbol{g}$ is the gravity vector, p is the pressure, t is the time, T is the temperature, $\boldsymbol{u}$ is the velocity vector, X is the mass fraction of the reactant, α is the thermal diffusivity, μ is the kinematic viscosity, and ρ is the mixture density. In the Boussinesq approximations, the density is taken to be constant everywhere except that in the body force term where it is approximated as a linear function of temperature,

$$\rho=\rho_0[1-\beta(T-T_0)] \tag{6}$$

with β being the thermal expansion constant. Strictly speaking, this expression is valid as long as the temperature range is small and the effects due to concentration variation are negligible.

The above equations are solved subject to the following conditions

$$(u_r,u_\theta)=(0,0)\quad T=\hat{T}=T_0,\quad X=X_0\quad \text{at}\quad t=0, \tag{7}$$

$$(u_r,u_\theta)=(0,\gamma),\quad T=\hat{T},\quad \kappa\frac{\partial T}{\partial r}-\hat{\kappa}\frac{\partial \hat{T}}{\partial r}=\Delta H_r k''\rho X_s^n,$$

$$D\frac{\partial X}{\partial r}=k''X_s^n,\quad \text{at}\quad r=1 \tag{8}$$

$$(u_r,u_\theta)=[1+\phi\sin(2\pi\omega_f t)](\cos\theta,-\sin\theta),$$

$$T=T_0,\quad X=1,\quad \text{at}\quad r\to\infty \tag{9}$$

where the rate coefficient, k'' is given by the Arrhenius law of the form (Carberry, 1976)

$$k''=k_0\exp\left(-\frac{E_a}{R_g T}\right), \tag{10}$$

where E_a is the activation energy, k_0 is a pre-exponential factor, R_g is the universal gas constant, and ΔH_r is the heat of reaction with positive $(-\Delta H_r)$ implying a heat-generating reaction.

For axisymmetric transport processes, it is more convenient to eliminate the pressure from the momentum equations by taking the curl of Eq. 2 and express the resulting in terms of the vorticity and a stream function. Thus,

$$\frac{\partial\zeta}{\partial t}-\frac{Re}{2r}J(\psi,\zeta)=\nabla^2\zeta-\frac{Gr}{4Re}$$

$$\times\left[\cos(\theta+\delta)\frac{\partial T}{\partial r}-\frac{\sin(\theta+\delta)}{r}\frac{\partial T}{\partial\theta}\right], \tag{11}$$

$$\nabla^2\psi=\zeta, \tag{12}$$

$$Pr\frac{\partial T}{\partial t}-\frac{RePr}{2r}J(\psi,T)=\nabla^2 T, \tag{13}$$

$$Sc\frac{\partial X}{\partial t}-\frac{ReSc}{2r}J(\psi,X)=\nabla^2 X, \tag{14}$$

$$Pr\frac{\partial \hat{T}}{\partial t}=\Phi_\alpha\nabla^2\hat{T}, \tag{15}$$

where the stream function ψ introduced above is related to the velocity by

$$\boldsymbol{u}=\frac{\boldsymbol{e}_r}{r}\frac{\partial\psi}{\partial\theta}-\boldsymbol{e}_\theta\frac{\partial\psi}{\partial r}. \tag{16}$$

Note that in the process to cast the foregoing equations in nondimensional form, the stream function has been made dimensionless by RU_∞, the rotational speed by U_∞, the time by R^2/ν, the temperature by T_0, and the radial coordinate by the cylinder radius R. The dimensionless groups Gr, Pr, Re, and Sc are known as the Grashof, Prandtl, Reynolds, and Schmidt numbers, respectively. Φ_α is the ratio of thermal diffusivities of the solid to the fluid.

With respect to the dimensionless quantities, the initial and boundary conditions now become:

At $t=0$

$$\psi=0,\quad T=1,\quad \hat{T}=1,\quad X=1. \tag{17}$$

At the cylinder surface, $r=1$

$$\psi=0,\quad \frac{\partial\psi}{\partial r}=-\Gamma,\quad T=\hat{T}, \tag{18a}$$

$$\frac{\partial T}{\partial r}-\Phi_\kappa\frac{\partial\hat{T}}{\partial r}=(\chi_1 D\ddot{a})X_s^n\exp\left[-\frac{\chi_2}{T_s}\right],$$

$$\frac{\partial X}{\partial r}=D\ddot{a}X_s^n\exp\left[-\frac{\chi_2}{T_s}\right]. \tag{18b}$$

At the free-stream, $r\to\infty$

$$\psi=[1+\phi\sin(2\pi\Omega_f t)]r\sin\theta,\quad T=1,\quad X=1, \tag{19}$$

where Ω_f and $D\ddot{a}$ are the Strouhal and the Damköhler numbers, respectively. These dimensionless groups and the parameters χ_1 and χ_2 appearing in Eq. 18b have been defined as

$$\Omega_f=\frac{\omega_f}{U_\infty/R},\quad D\ddot{a}=\frac{Rk_0}{D},\quad \chi_1=\frac{\Delta H_r D}{\alpha c_p T_0}\quad \chi_2=\frac{E_a}{R_g T_0}. \tag{20}$$

Methods of Solution

Temporal and spatial discretizations

Following Nguyen et al. (1995), time discretization will be accomplished by the use of the second-order Adams-Bashforth method and the first-order backward Euler method for the convection and diffusion terms, respectively. In so doing, the semi-discrete analogs of the flow and the energy equations are the same as before and since the species equation is similar to the energy equation, neither is repeated here.

For the spatial discretization, the stream function, vorticity, temperature and the concentration are represented by truncated Fourier expansions of the form

$$\begin{Bmatrix}\psi\\ \omega\\ T\\ \hat{T}\\ X\end{Bmatrix}=\frac{1}{2}\begin{Bmatrix}F_0(r)\\ G_0(r)\\ H_0(r)\\ \hat{H}_0(r)\\ Q_0(r)\end{Bmatrix}+\sum_{i=1}^{I}\begin{Bmatrix}F_i(r)\\ G_i(r)\\ H_i(r)\\ \hat{H}_i(r)\\ Q_i(r)\end{Bmatrix}\cos(i\theta)+\begin{Bmatrix}f_i(r)\\ g_i(r)\\ h_i(r)\\ \hat{h}_i(r)\\ q_i(r)\end{Bmatrix}\sin(i\theta), \tag{21}$$

where $\{f_i\}$, $\{F_i\}$, $\{g_i\}$, $\{G_i\}$, $\{h_i\}$, $\{H_i\}$ $\{\hat{h}_i\}$, $\{\hat{H}_i\}$, $\{q_i\}$ and $\{Q_i\}$ are ten sets of unknown functions to be determined and I is the number of Fourier modes. By substituting these expressions into Eqs. 11 to 15 and equating terms having a common factor in sin $(i\theta)$ and cos $(i\theta)$ yields equations for the expansion coefficients

$$-\frac{d}{dr}\left(r\frac{dH_i^{k+1}}{dr}\right)+\left[\frac{Pr}{\Delta t}r+\frac{i^2}{r}\right]H_i^{k+1}=\frac{Pr}{\Delta t}rH_i^k+\frac{RePr}{8}[3SH_i^k-SH_i^{k-1}], \tag{22}$$

$$-\frac{d}{dr}\left(r\frac{dh_i^{k+1}}{dr}\right)+\left[\frac{Pr}{\Delta t}r+\frac{i^2}{r}\right]h_i^{k+1}=\frac{Pr}{\Delta t}rh_i^k+\frac{RePr}{8}[3Sh_i^k-Sh_i^{k-1}], \tag{23}$$

$$-\frac{d}{dr}\left(r\frac{dQ_i^{k+1}}{dr}\right)+\left[\frac{Sc}{\Delta t}r+\frac{i^2}{r}\right]Q_i^{k+1}=\frac{Sc}{\Delta t}rQ_i^k+\frac{ReSc}{8}[3SQ_i^k-SQ_i^{k-1}], \tag{24}$$

$$-\frac{d}{dr}\left(r\frac{dq_i^{k+1}}{dr}\right)+\left[\frac{Sc}{\Delta t}r+\frac{i^2}{r}\right]q_i^{k+1}=\frac{Sc}{\Delta t}rq_i^k+\frac{ReSc}{8}[3Sq_i^k-Sq_i^{k-1}], \tag{25}$$

$$-\Phi_\alpha\frac{d}{dr}\left(r\frac{d\hat{H}_i^{k+1}}{dr}\right)+\left[\frac{Pr}{\Delta t}r+\Phi_\alpha\frac{i^2}{r}\right]\hat{H}_i^{k+1}=\frac{Pr}{\Delta t}r\hat{H}_i^k, \tag{26}$$

$$-\Phi_\alpha\frac{d}{dr}\left(r\frac{d\hat{h}_i^{k+1}}{dr}\right)+\left[\frac{Pr}{\Delta t}r+\Phi_\alpha\frac{i^2}{r}\right]\hat{h}_i^{k+1}=\frac{Pr}{\Delta t}r\hat{h}_i^k, \tag{27}$$

where the convection terms are given in Nguyen et al. (1995). Note that only equations for the temperature and concentration expansion coefficients were reproduced above in order to clarify the decoupling strategy of the temperature-concentration coupling at the fluid-solid interface to be discussed in the next subsection. Those associated with the stream function and vorticity could be found in Nguyen et al. (1995) and were therefore omitted.

To complete the discretization process, a Galerkin-based spectral element method with Lagrangian interpolants is used for radial discretization so that Eqs. 22 to 27 become systems of algebraic equations whose solution can be obtained by a linear equation solver. For detailed information about the spectral element method, refer to the original work of Patera (1984) and that of Nguyen et al. (1995) where the method was applied to a mixed convection problem of similar physical setting, but with a passive fluid.

Interface temperature-concentration decoupling

Even though the semidiscrete form of the energy and species equations are linear, the couplings at the interface necessitate some sort of iteration. Alternatively, one can decouple those two equations using the influence matrix technique which was originally proposed for handling the difficulty of specifying the boundary conditions for the vorticity transport equations. The key idea of this procedure is, based on the superposition principle, to decompose the solution as follows

$$\begin{Bmatrix}H_i^{k+1}\\ \hat{H}_i^{k+1}\\ Q_i^{k+1}\end{Bmatrix}=\begin{Bmatrix}\Theta_0\\ \hat{\Theta}_0\\ \Xi_0\end{Bmatrix}+H_{s,i}\begin{Bmatrix}\Theta_1\\ \hat{\Theta}_1\\ 0\end{Bmatrix}+Q_{s,i}\begin{Bmatrix}0\\ 0\\ \Xi_1\end{Bmatrix}, \tag{28}$$

where $H_{s,i}$ and $Q_{s,i}$ are, as they turn out, the unknown surface temperature and concentration associated with the i-th cosine component to be determined. The auxiliary functions appearing in Eq. 28 are the solutions of the following elementary problems

$$\left.\begin{aligned}&-\frac{d}{dr}\left(r\frac{d\Theta_1}{dr}\right)+\left[\frac{Pr}{\Delta t}r+\frac{i^2}{r}\right]\Theta_1=0\\ &\Theta_1(1)=1+\delta_{0i}\quad\text{and}\quad\Theta_1(\infty)=0\end{aligned}\right\}, \tag{29}$$

$$\left.\begin{aligned}&-\Phi_\alpha\frac{d}{dr}\left(r\frac{d\hat{\Theta}_1}{dr}\right)+\left[\frac{Pr}{\Delta t}r+\Phi_\alpha\frac{i^2}{r}\right]\hat{\Theta}_1=0\\ &\hat{\Theta}_1(0)=0\quad\text{and}\quad\hat{\Theta}_1(1)=1+\delta_{0i}\end{aligned}\right\}, \tag{30}$$

$$\left.\begin{aligned}&-\frac{d}{dr}\left(r\frac{d\Xi_1}{dr}\right)+\left[\frac{Sc}{\Delta t}r+\frac{i^2}{r}\right]\Xi_1=0\\ &\Xi_1(1)=1+\delta_{0i}\quad\text{and}\quad\Xi_1(\infty)=0\end{aligned}\right\}, \tag{31}$$

$$-\frac{d}{dr}\left(r\frac{d\Theta_0}{dr}\right)+\left(\frac{Pr}{\Delta t}r+\frac{i^2}{r}\right)\Theta_0 = \frac{Pr}{\Delta t}rH_i^k+\frac{RePr}{8}[3SH_i^k-SH_i^{k-1}] \quad \Theta_0(0)=0 \text{ and } \Theta_0(\infty)=0 \Bigg\}, \tag{32}$$

$$-\Phi_\alpha\frac{d}{dr}\left(r\frac{d\hat{\Theta}_0}{dr}\right)+\left(\frac{Pr}{\Delta t}r+\Phi_\alpha\frac{i^2}{r}\right)\hat{\Theta}_0=\frac{Pr}{\Delta t}r\hat{H}_i^k \quad \hat{\Theta}_0(0)=0 \quad \text{and} \quad \hat{\Theta}_0(1)=0 \Bigg\}, \tag{33}$$

$$-\frac{d}{dr}\left(r\frac{d\Xi_0}{dr}\right)+\left(\frac{Sc}{\Delta t}r+\frac{i^2}{r}\right)\Xi_0 = \frac{Sc}{\Delta t}rQ_i^k+\frac{ReSc}{8}[3SQ_i^k-SQ_i^{k-1}] \quad \Xi_0(0)=0 \text{ and } \Xi_0(\infty)=0 \Bigg\}, \tag{34}$$

Upon enforcing Eq. 28 to satisfy the surface conditions, there results two nonlinear equations

$$\left(\frac{d\Theta_1}{dr}-\Phi_\kappa\frac{d\hat{\Theta}_1}{dr}\right)H_{s,i}-(\chi_1 D\ddot{a})S_i+\frac{d\Theta_0}{dr}-\Phi_\kappa\frac{d\hat{\Theta}_0}{dr}=0, \tag{35}$$

$$\frac{d\Xi_1}{dr}Q_{s,i}-D\ddot{a}S_i+\frac{d\Xi_0}{dr}=0, \tag{36}$$

in which S_i is the i-th Fourier coefficient of the cosine function of the source term, i.e.,

$$X_s^n\exp\left(-\frac{\chi_2}{T_s}\right)=\frac{1}{2}S_0+\sum_{i=1}^{I}S_i\cos(i\theta)+s_i\sin(i\theta), \tag{37}$$

where T_s and X_s may be expressed in terms of $H_{s,i}$, $h_{s,i}$, $Q_{s,i}$, and $q_{s,i}$ as

$$T_s=\frac{1}{2}H_{s,0}+\sum_{i=1}^{I}H_{s,i}\cos(i\theta)+h_{s,i}\sin(i\theta), \tag{38}$$

$$X_s=\frac{1}{2}Q_{s,0}+\sum_{i=1}^{I}Q_{s,i}\cos(i\theta)+q_{s,i}\sin(i\theta). \tag{39}$$

Similarly, the procedure can be repeated for other components, thereby constituting a system of nonlinear equations in $4I+2$ unknowns which must be solved iteratively. The Newton-Raphson method is adopted in this study with the Jacobian evaluated numerically. This requires solving a system of equations repeatedly until the solution is within the prescribed tolerance, which is set at 10^{-4} for all the simulations reported in the next section. Note the influence matrix technique is an exact procedure that does not involve any approximation. Though somewhat tedious, it provides an efficient means to isolate the interfacial couplings from the governing differential equations so that the interfacial parameters can be solved separately. Because the system of equations for these parameters is usually small, this procedure would lead to a saving of execution time and enhance the robustness of the numerics.

Results and Discussion

In a related study (Nguyen et al., 1995), several tests were carried out to validate the code wherein the above equations were implemented and a good agreement with literature results was demonstrated. Thus, we shall now concentrate our effort to understand the underlying mechanisms of heat and mass transfer in the presence of a reaction at the solid-fluid interface. We do so by organizing the remainder of the discussion by first looking at the temporal development of the flow, temperature, concentration, and vorticity fields. Then, we shall examine the local response of temperature and concentration at the surface and the time variations of their averaged values, and finally, we shall conduct a parametric study to examine the surface performance of catalytic surface under various conditions. Unless otherwise specified, values of the model parameters are those listed in Table 1. All the calculations are done using $\Delta t=10^{-4}$, $r_\infty=100$, $I=25$, $E=40$, $\hat{E}=15$, and $N^e=2$. The size of the elements varies according to $\Delta r^{e+1}=1.3\Delta r^e$ in the outer flow and $\Delta\hat{r}^{e+1}=0.8\Delta\hat{r}^e$ inside the cylinder, respectively. Our studies show that if $I=30$ and $E=50$ are used whenever convection is enhanced, then the solutions are free of grid dependence. This is the case when the main flow is aided by buoyancy-induced motion or when Pr or Sc is greater than 2.

Figure 2 illustrates the qualitative structure of the flow, temperature, and concentration fields at $t=0.01$, 0.05, 0.1, 0.5, and 2.0 for the case of uniform shear flow past a stationary circular cylinder with heat generated along the surface as a result of the chemical reaction with $\Gamma=0$. As one can see clearly, diffusion is dominated in the early stage of the transport process as evidenced by the symmetry about the equatorial plane of the flow and about the center of the temperature and concentration. Such symmetries are gradually destroyed in time as convection becomes more intensified as manifested by the appearance of a secondary flow in the form of eddies in the wake. Once formed, these eddies grow in size in both spanwise and streamwise directions. These developments lead to a distortion of the temperature and concentration contours from being radially symmetric to those shown in Figures 2b to 2e. Consequently, the surface temperature and concentration become nonuniform and this, in turn, results in an unsymmetric distribution of temperature inside the cylinder such that the isotherms behave very much like straight lines at large times. While mass transport resistance is infinite within the cylinder, the concentration field in the

Table 1. Values of Simulation Parameters

Parameter	Definition	Value	Parameter	Definition	Value
Re	$2U_\infty R/\nu$	100	χ_1	$\Delta H_r D/\alpha c_p T_0$	-10.0
Gr	$8g\beta T_0 R^3/\nu^2$	0	χ_2	$E_a/R_g T_0$	1.0
Pr	ν/α	0.73	ϕ	—	0.0
$D\ddot{a}$	Rk_0/D	5.0	Ω_f	$\omega_f R/U_\infty$	0.0
Sc	ν/D	2.0	Γ	γ/U_∞	0.2
Φ_α	$\hat{\alpha}/\alpha$	10.0	δ	—	0.0
Φ_κ	$\hat{\kappa}/\kappa$	5.0	n	—	1.7

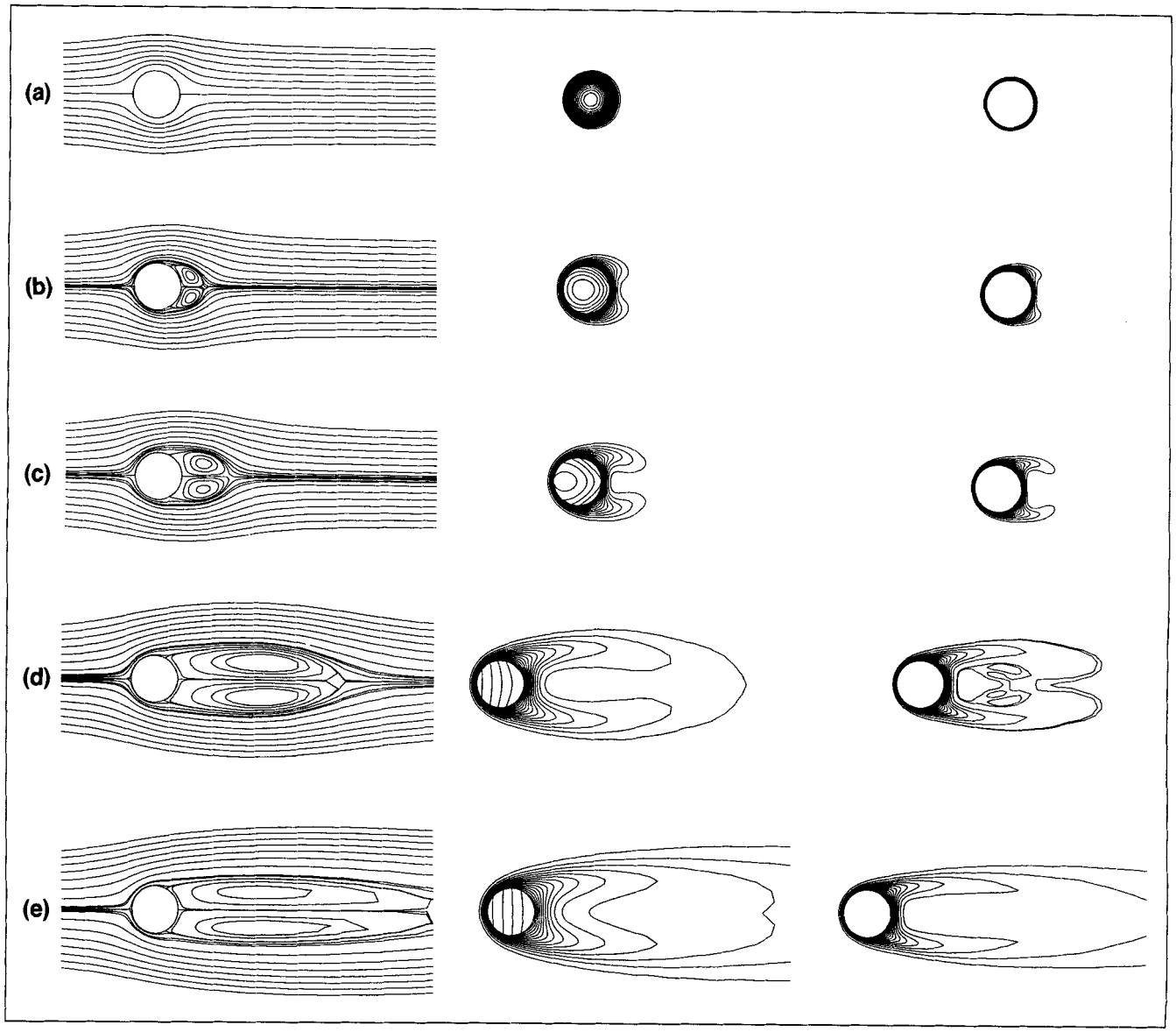

Figure 2. Contour maps of stream function (left), temperature (center), and mass fraction (right) for without rotation.

(a) $t = 0.01$; (b) $t = 0.05$; (c) $t = 0.1$; (d) $t = 0.5$; (e) $t = 2.0$.

fluid phase is very similar to that of the temperature in structure except the concentration plume which seems to be narrower and longer in the direction normal to and parallel to, respectively, the free stream velocity. This is due to the fact that thermal diffusion is nearly three times faster than mass diffusion as reflected by the Schmidt number of 2.

The experiment indicates that for $Re = 100$, a pattern of well organized vortices formed and subsequently shed behind the cylinder. The simulations do not show this instability without supplying an external perturbation. To study heat and mass transport in this flow regime, a perturbation in the form of cylinder rotation is introduced so as to trigger the shedding phenomena. The results are demonstrated in Figure 3 for $\Gamma = 0.2$. Again, at small times, the contour maps of the stream function, temperature, and concentration are essentially the same as if rotation is absent. As discussed earlier, this period is controlled by diffusive mechanisms and is characterized by isotherms and isoconcentrations of circular shape. Soon after this period, convection begins to take control and eddies of different sizes are formed and detached from the surface as seen in the stream lines. Correspondingly, the contours of temperature and concentration in the upper half and bottom half are no longer images of each other. When shedding happens, the detached vortex carries with it fluid particles with temperature and concentration different from those of the surrounding fluid as it travels downstream. Despite the cylinder rotation that has produced totally different flow, temperature, and concentration fields from those without rotation, the internal temperature pattern remains very much unchanged.

Figures 4a and 4b show the variations of the temperature and concentration, respectively, for the two cases discussed above. As displayed, the profiles with and without rotation seem to be somewhat similar and are much more so for tem-

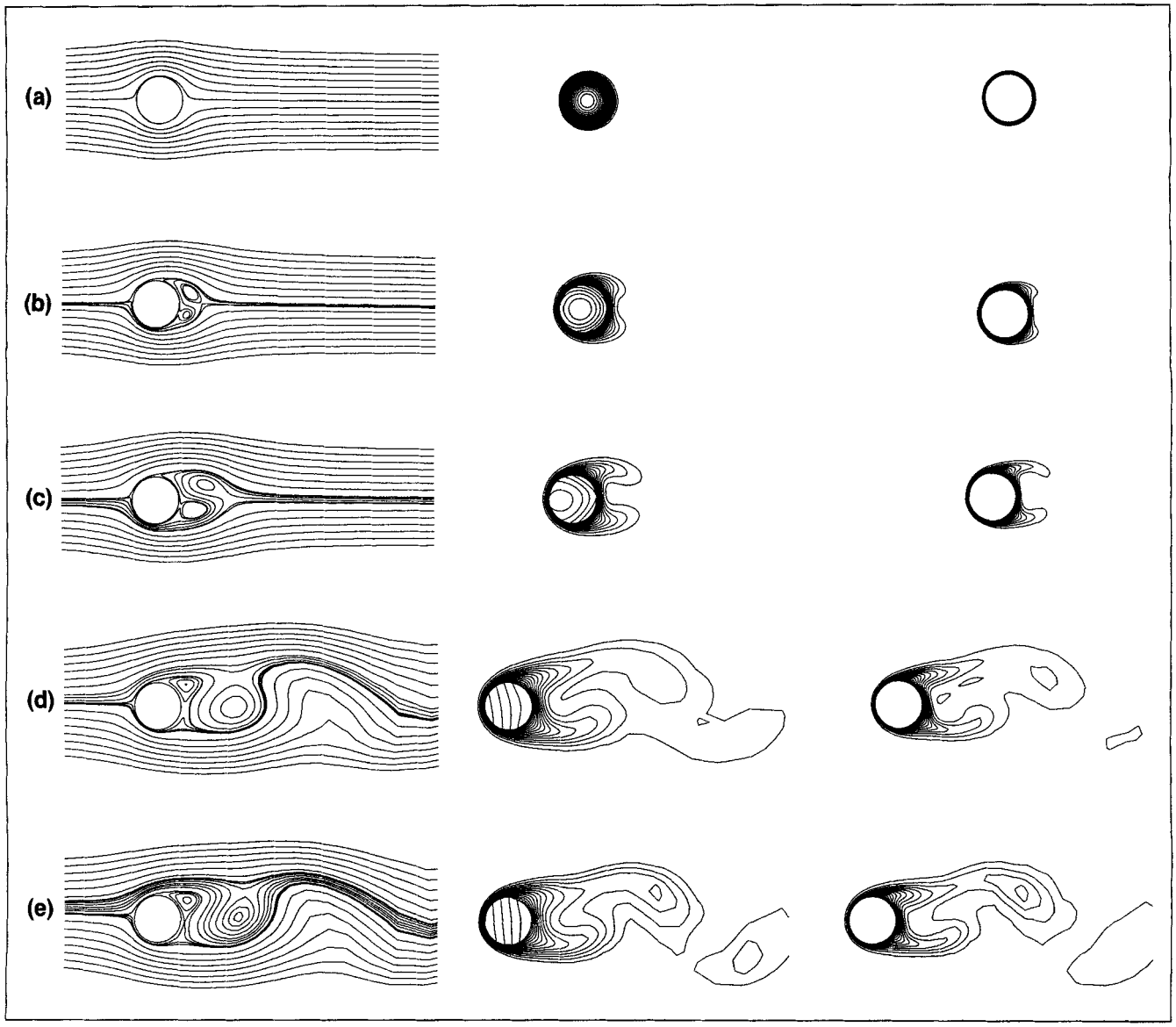

Figure 3. Contour maps of stream function (left), temperature (center), and mass fraction (right) for the case with rotation.

(a) $t = 0.01$; (b) $t = 0.05$; (c) $t = 0.1$; (d) $t = 0.5$; (e) $t = 2.0$.

perature than concentration. This is primarily due to the Schmidt number being 2 as opposed to the Prandtl number being 0.73. Though the similarity of surface concentration profiles with and without rotation is not as close as for temperature, the difference is limited to the wake region and attributed to the growth and the detachment of eddies. Regardless of whether rotation is present or not, it is clear that the surface temperature and concentration are far from being uniform, especially in the later stages of the evolution. Such a strong nonuniformity necessitates a conjugate analysis that requires solution of coupled equations as pursued in this investigation. Note that without rotation the surface temperature and reactant concentration seem to reach their steady-state solution at $t \approx 0.5$ since the curves at $t = 0.5$ and $t = 2.0$ are overlapped while those with rotation seem to be oscillating owing to the shedding event.

In Figure 5 the average surface temperature and reactant concentration are plotted as functions of time for five different values of rotation velocity. In general, the curves reveal that an increase in rotation speed causes a decrease in surface temperature and this causes the reaction to slow down and leaves more of species A unreacted, hence yielding higher reactant concentration. Unlike the surface temperature which is affected very little by the vortex shedding, the reactant concentration is more sensitive as the curves exhibit a higher magnitude of periodic oscillations. This is, once again, due to Schmidt number greater than unity.

To determine the performance of the surface, a parametric study was conducted to quantify the effectiveness factor defined as the ratio of the amount reacted along the reacting surface to that if the surface is maintained at the bulk fluid conditions, i.e.,

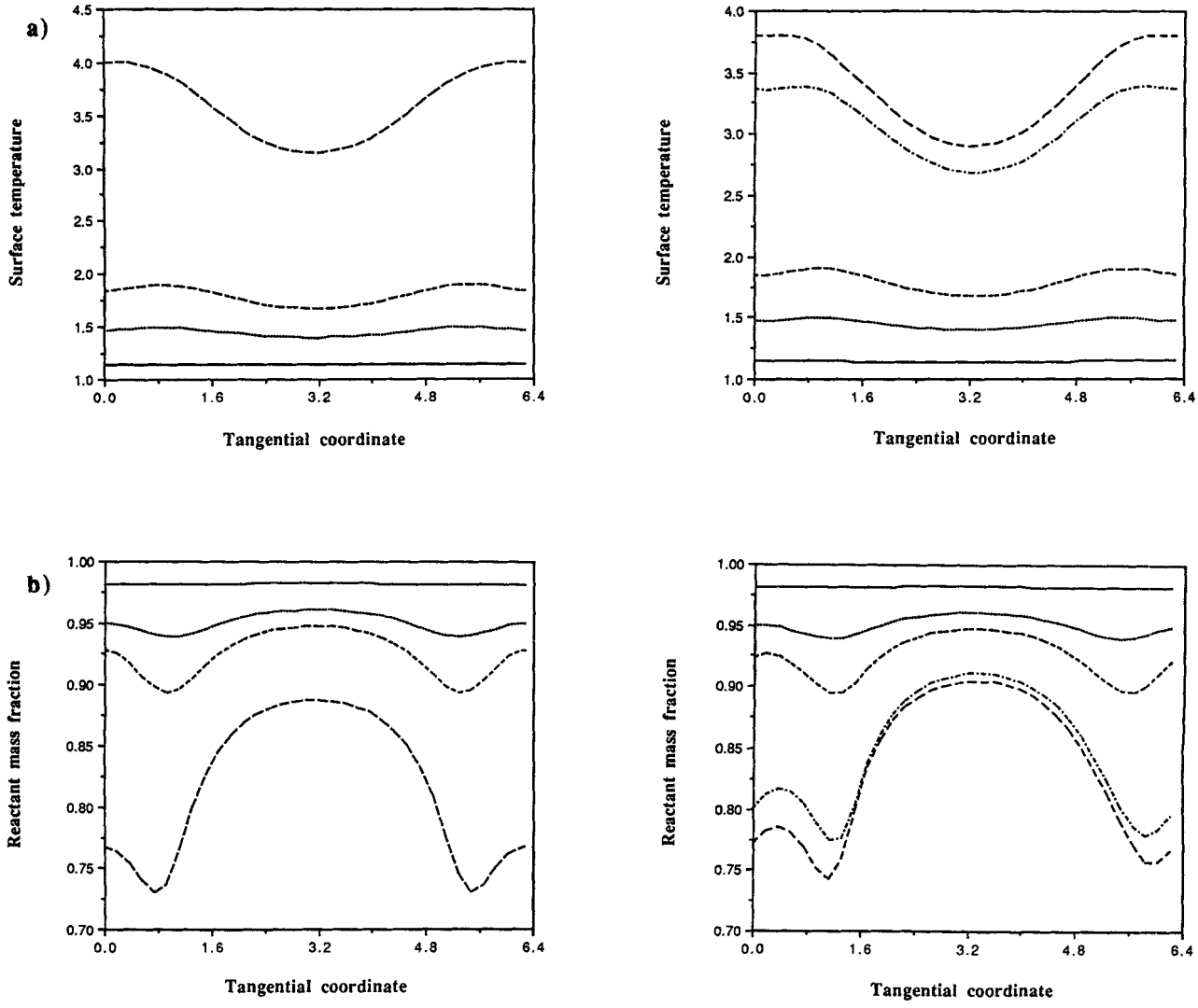

Figure 4. Evolution of surface quantities without rotation (left) and with rotation (right).

(a) Temperature; (b) reactant mass fraction.

$$\eta = \frac{1}{2\pi k''_{\infty} c^n_{\infty}} \int_0^{2\pi} k'' c^n d\theta$$

$$= \frac{1}{2\pi} \int_0^{2\pi} e^{(1-1/T_s)} X_s^n d\theta,$$

which is, in general, a function of the parameters listed in Table 1. Figures 6a to 6j provide the time history of the effectiveness factor for several combinations of the parameters in which one parameter is varied at a time. In Figure 6a it is quite obvious that the higher the Reynolds number, the higher the effectiveness factor. At low Reynolds number, the curve attains a peak and drops off thereafter; however, this trend tends to diminish as the Reynolds number increases and the curve increases monotonically with the asymptotic value reached in a short period of time. The Grashof number varies with the gravity acceleration vector, which is perpendicular to the free stream velocity for all cases (Figure 6b). As anticipated, the presence of the buoyancy force does indeed enhance the performance of the catalytic surface but may alter the shedding frequency. For Figure 6c, an increase in the Prandtl number results in a decrease in the performance. This may be explained by the fact that at larger *Pr*, heat is more readily diffused from the surface of the cylinder, which is thus cooler, leading to a slowdown of the reaction. For Schmidt number effects, Figure 6d, the trend is opposite since a higher Schmidt number implies that the mass diffusivity of the fluid is reduced, thereby increasing the local mass concentration gradient and maintaining a larger mass fraction along the cylinder's surface.

Unlike the previous four cases where a definite trend can easily be identified, the case of varying Damköhler number shown in Figure 6e reveals an irregular behavior. For the range of values (from 1 to 10) investigated in this study, there exists a critical Damköhler number below which the effectiveness factor is a monotonic increasing function of time. Above the number, it increases rapidly to a maximum value and drops off to a lower asymptotic value. By further refinement of the effects, its critical value was found to be about 5.5. This behavior is speculated to be due to the nonlinear

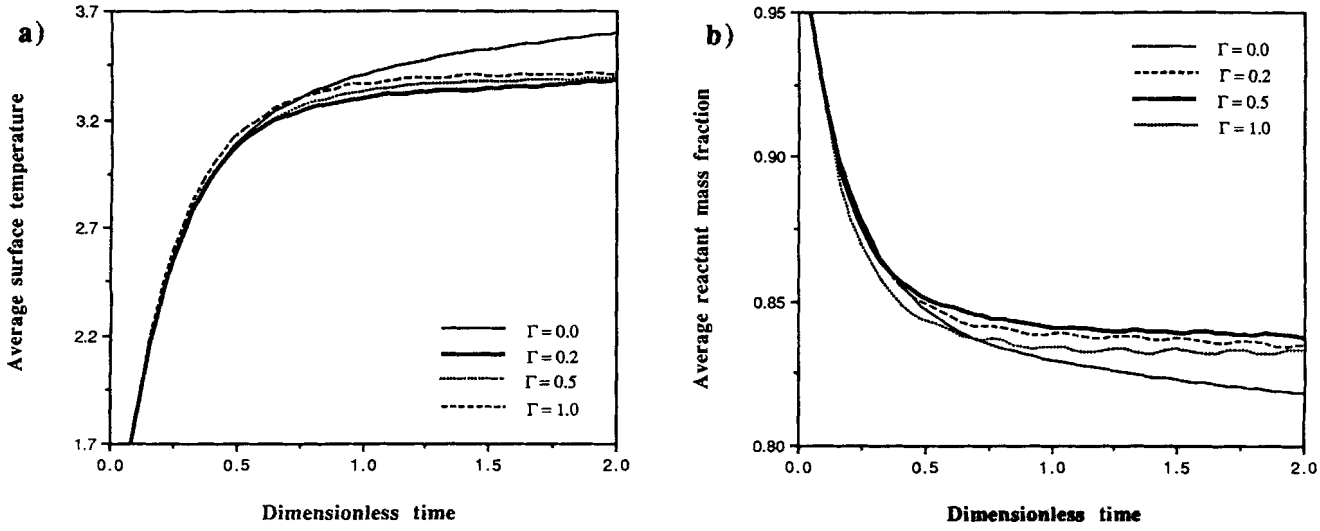

Figure 5. History of surface-averaged quantities.

(a) Temperature; (b) reactant mass fraction.

dependence of the rate expression on temperature and concentration. Figure 6f shows how the reaction rate order n affects the effectiveness factor. Because a large value of n implies a slow reaction and vice versa, the larger the value of n the lower the effectiveness factor. Like Figure 6e, a peak is observed for n less than about 1.6.

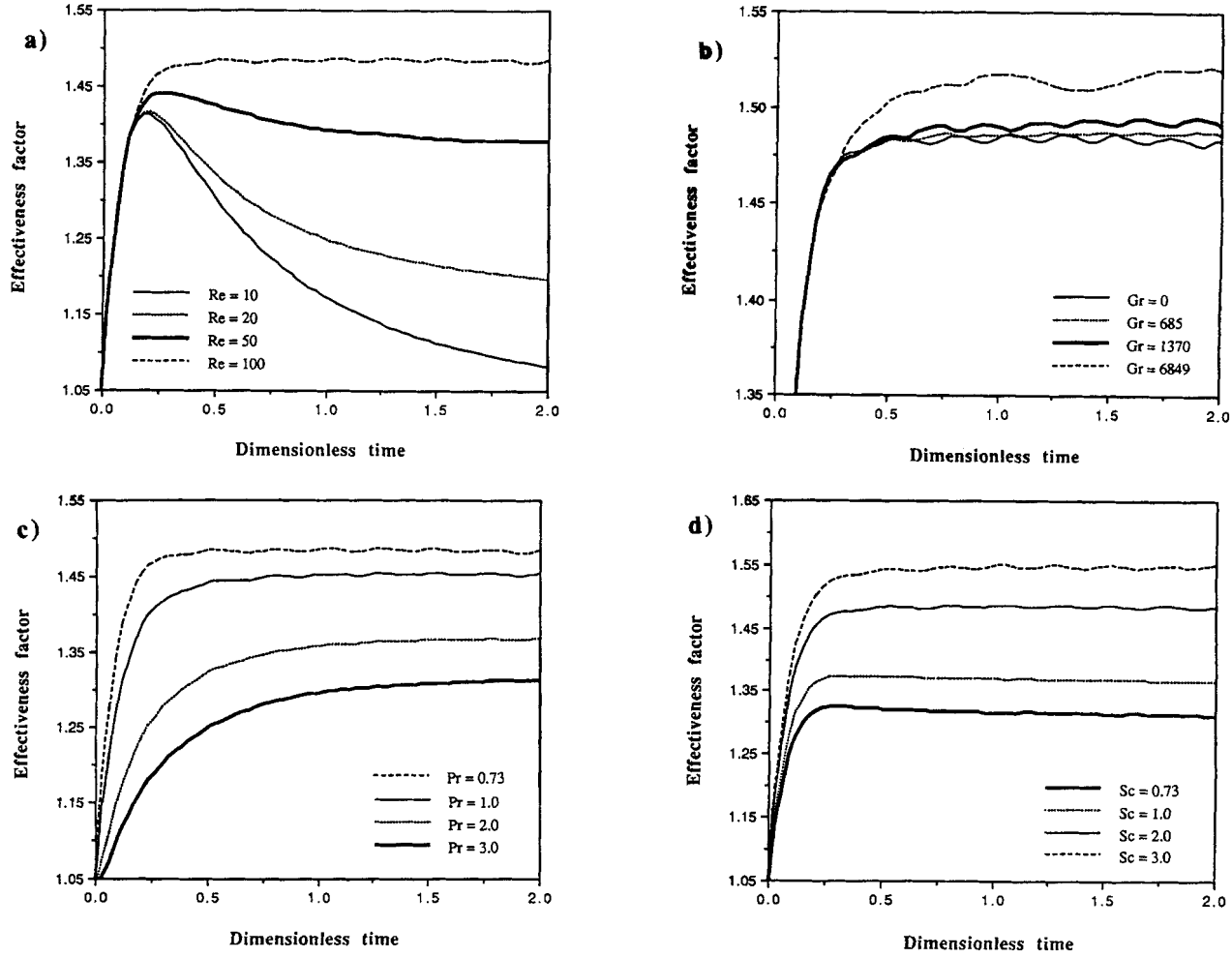

Figure 6. Effectiveness factor.

(a) *Re* varying; (b) *Gr* varying; (c) *Pr* varying; (d) *Sc* varying.

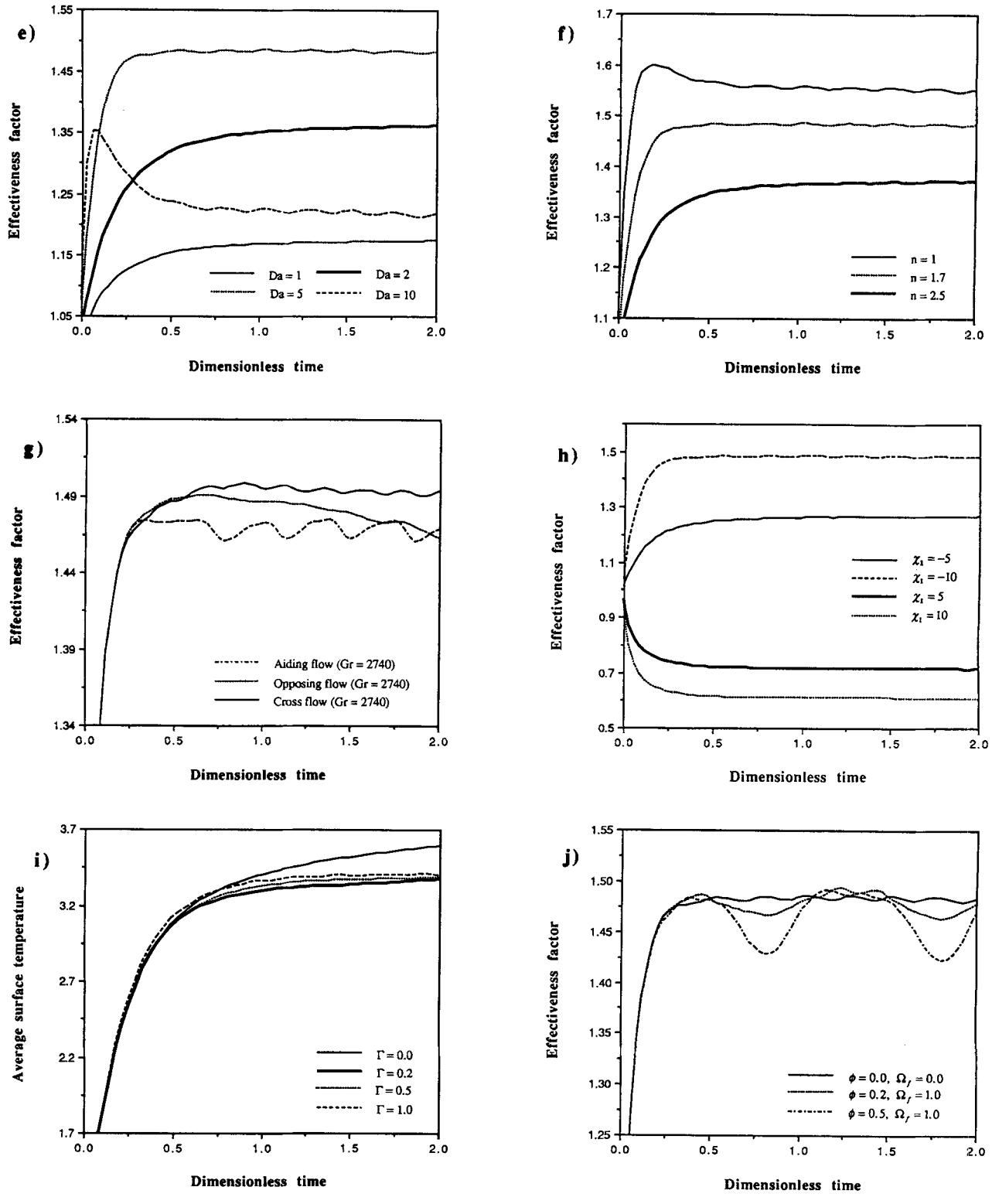

Figure 6. Effectiveness factor.

(e) *Da* varying; (f) n varying; (g) δ varying; (h) χ_1 varying; (i) Γ varying; (j) ϕ varying.

Figure 6g shows the effects of the direction of gravity on the effectiveness factor. Here, it is worthwhile to note that when the main flow is aided by the buoyancy force ($\delta = 0.5\pi$) the effectiveness factor decreases. Figure 6h presents the effects of heat liberated or consumed during the transport process. For exothermic reactions, the heat release from the reaction causes an elevation of temperature along the cylinder surface which, in turn, intensifies the reaction. Thus, the

greater the heat of the reaction the higher the effectiveness factor. On the contrary, endothermic reactions require heat to sustain the reaction and the trend is therefore reversed.

Finally, in Figure 6i it is observed that the spinning motion of the cylinder has little influence on the effectiveness factor and that its presence causes the catalytic surface to perform poorly. Figure 6j demonstrates the response of the surface under flow pulsation. Although the fluctuations in the free stream velocity lead to oscillations in the effectiveness factor, the overall performance may not be desirable, hence flow pulsation is not a recommended means of increasing the surface performance.

Conclusions

The problem of mixed convection heat and mass transfer, including internal conduction inside the cylinder in the presence of a surface reaction of arbitrary order, is investigated using a Fourier-spectral element method. Results on the temporal development of the flow, temperature, and concentration fields, as well as the evolution of the surface temperature and concentration, have been presented to show the global and local effects due to vortex shedding. Surface effectiveness has also been quantified to illustrate the catalytic performance under a variety of conditions. These results have led to the following conclusions:

- When vortex shedding occurs, the temperature and concentration fields become asymmetrical about the horizontal axis and the detachment of vortices from the cylinder's surface leads to dispersed fluid particles with higher temperature and lower reactant concentration than those in the surrounding fluid.
- The shedding phenomena causes the temperature along the surface of the cylinder to be elevated which, in turn, leads to lower reactant concentration. The profile shapes of the surface temperature and concentration, especially in the wake, are also modified with the latter being more pronounced because convection is more influential in the concentration field for the cases examined in this study.
- The fluctuations appearing in the time history curves are a direct consequence of the shedding event.
- Regardless of whether there is vortex shedding or not, the internal isotherms are very much straight lines perpendicular to the free stream velocity.
- All the parameters considered in the parametric study, Re, Gr, Pr, Sc, $Dä$, n, δ, χ_1, and ϕ, reveal a strong influence on the surface performance, except the cylinder rotation parameter Γ. For the Damköhler number and the reaction order, there exists a critical value at which the shape of the effectiveness profile changes from being monotonic to a skewed bell shaped curve.

Acknowledgment

This work is performed under the auspices of the U.S. Department of Energy, contract DE-AC07-94ID13223, and is supported through the INEL Long-Term Research Initiative in Computational Mechanics.

Notation

$\hat{D}_{i,i'}^{(\ell)}$ = Chebyshev matrix for ℓ-th derivative
f_i, F_i = sine and cosine components of stream function, respectively
g_i, G_i = sine and cosine components of vorticity, respectively
h_i, H_i = sine and cosine components of temperature, respectively

Greek letters

δ = angle between free stream velocity direction and gravity direction
ΔH_r = heat of reaction
Δt = time increment
ζ = vorticity
η = effectiveness factor
θ = angular coordinate
κ = thermal conductivity

Subscripts

s = value at the catalytic surface
∞ = value at the free-stream
0 = initial value

Superscripts

k = time level
n = reaction order
q_i, Q_i = sine and cosine components of mass fraction, respectively
r = radial coordinate
R_g = universal gas constant

Literature Cited

Basic, A., and M. P. Dudukovic, "A Series Solution for Mass Transfer in Laminar Flow with Surface Reaction," *AIChE J.*, **37**, 1341 (1991).

Bauer, H., "Diffusion, Convection and Chemical Reaction in a Channel," *Int. J. Heat Mass Transf.*, **19**, 479 (1976).

Carberry, J. J., *Chemical and Catalytic Reaction Engineering*, McGraw-Hill, New York (1976).

Chung, P. M., "Chemically Reacting Nonequilibrium Boundary Layers," *Adv. in Heat Transf.*, **2**, 109 (1965).

Finlayson, B. A., "Hysteresis and Multiplicity in Wall-Catalyzed Reactors," *Chemical Reaction Engineering — Houston*, Chap. 9, V. W. Weekman and D. Luss, eds., Amer. Chem. Soc. (1978).

Ghez, R., "Mass Transport and Surface Reactions in Leveque's Approximation," *Int. J. Heat Mass Transf.*, **21**, 745 (1978).

Hudson, J. L., "Diffusion with Consecutive Heterogeneous Reactions," *AIChE J.*, **11**, 943 (1965).

Lyczkowski, R. W., G. Gidaspow, and C. W. Solbrig, "Consecutive Surface Reactions in Fully Developed Laminar and Turbulent Flow," *AIChE J.*, **17**, 197 (1971).

Nguyen, H. D., S. Paik, and R. W. Douglass, "Unsteady Mixed Convection about a Rotating Circular Cylinder with Small Fluctuations in the Free-Stream Velocity," *Int. J. Heat Mass Transf.*, accepted (1995).

Patera, A. T., "A Spectral Element Method for Fluid Dynamics: Laminar Flow in Channel Expansion," *J. Comput. Phys.*, **54**, 468 (1984).

Riley, N., "Surface Reactions in Similar Boundary Layers," *Quart. J. Mech. Appl. Math.*, **25**, 273 (1972).

Rosner, D. E., "Convective Diffusion as an Intruder in Kinetic Studies of Surface Catalyzed Reactions," *AIAA J.*, **2**, 593 (1964).

Smith, T. G., and J. J. Carberry, "Design and Optimization of a Tube-Wall Reactor," *Chem. Eng. Sci.*, **30**, 221 (1975).

Solbrig, C. W., and D. Gidaspow, "Turbulent Mass Transfer with an Arbitrary Order Surface Reaction in a Flat Duct," *Int. J. Heat Mass Transf.*, **11**, 155 (1968).

Manuscript received June 16, 1995, and revision received Aug. 24, 1995.